

Short Communication

## Study on the Corrosion Behavior of Q345B Steel as Grounding Electrode Material in UHVDC System Based on Electrochemical and Immersion Experiment

Changsheng Liu, Sha Wang\*

Department of Electrical & Electronic Engineering, Hubei University of Technology Engineering and Technology College, Hubei WuHan, 430068, China

\*E-mail: [swang\\_hbut@126.com](mailto:swang_hbut@126.com)

Received: 18 July 2022 / Accepted: 25 August 2022 / Published: 10 October 2022

The corrosion caused by direct current was the main factor to result in the failure of grounding electrode in UHVDC (ultra-high voltage direct current) system. Compared with the severe corrosion caused by thousands of amperes flowing from the grounding electrode during the system failure, the corrosion of grounding electrode caused by electric field formed by the unbalanced current can not be ignored in normal operation, but there were little relevant reports and studies focusing on this condition. In this paper, the corrosion behavior of Q345B steel as grounding electrode material was studied under different direct current density of 0-1.5 A/cm<sup>2</sup> based on the electrochemical experiment and immersion experiment. The results showed that with the increase of direct current density ( $I_{DC}$ ), the corrosion potential ( $E_{corr}$ ), corrosion current density ( $I_{corr}$ ), corrosion rate and maximum pit depth showed the linear changing rules, namely  $E_{corr} = -0.0568 \cdot I_{DC} - 0.7338$  ( $R^2 = 0.8784$ ),  $I_{corr} = 33.69 \cdot I_{DC} - 4.3406$  ( $R^2 = 0.9649$ ), corrosion rate =  $0.0648 \cdot I_{DC} + 0.0047$  ( $R^2 = 0.9952$ ) and maximum pit depth =  $80.032 \cdot I_{DC} + 83.946$  ( $R^2 = 0.9554$ ), respectively. The coverage rate of corrosion products on the surface of Q345B steel gradually decreased, and the corrosion products changed from polygon to triangle, which can be described as  $Fe_2O_3$  ( $FeO(OH) \rightarrow Fe_2O_3 + H_2O$ ),  $FeO(OH)$  ( $4Fe + 3O_2 + 2H_2O \rightarrow 4FeO(OH)$ ) and  $FeCO_3$  ( $Fe + HCO_3^- \rightarrow FeCO_3 + H^+ + 2e^-$ ).

**Keywords:** Ultra-high voltage direct current transmission; Grounding electrode material; Q345B steel; Corrosion behavior; Electrochemistry

### 1. INTRODUCTION

The grounding electrode is a very important part of the DC (direct current) transmission engineering, which provides a path for the unbalanced current about 1% of the rated current to flow into the soil. Especially for the condition of transmission system, the rated current reaching thousands of amperes drains into soil, to make sure the safety of the system. As the number of UHVDC (ultra-

high voltage direct current) transmission projects increased year by year in China, the influence of direct current on grounding electrode corrosion becomes more and more prominent [1-4].

There have been a lot of reports on the influence of direct current on the corrosion behavior of carbon steel materials, which was also widely used for grounding electrode and pipeline [5-9]. The corrosion rate caused by the direct current on carbon steel in soil environment is closely related to the interference time and stray current density. The longer the current action time is, the greater the influence on corrosion rate is [10]. The corrosion behavior of carbon steel in soil can be measured by means of weight loss method, electrochemical testing, SEM (scanning electron microscope) and XRD (X-Ray diffraction) [11,12], and then the corresponding experimental data can be obtained.

Wang et al. studied the influence of direct current on corrosion characteristics of Q235 steel in Yingtan acid soil with water content of 30% and 40% by means of electrochemical impedance spectroscopy (EIS), weight loss method, SEM and XRD test [13]. They found that with the increase of direct current density, the capacitive arc of EIS curves decreased gradually, while the corrosion rate and the maximum pit depth increased. Doyle et al. studied the influence of direct current on the corrosion of ground material, including Q235 steel, Q235 galvanized steel and Cu in soil with different moisture content by means of EIS curves, polarization curve and weight loss method [14]. The research results showed that in the presence of direct current, the polarization resistance and charge transfer resistance of these three grounding materials decreased with the increase of water content [15], but the corrosion current density and weight loss rate increased, indicating that the direct current accelerated the corrosion process of grounding materials [16]. Cole et al. studied the corrosion potential and corrosion rate of Q235 and Q345 steels in different soil environments by applying external direct current density through field tests, and obtained the corrosion characteristics of the two steels in different soil environments [17]. It was found that the corrosion potential of carbon steel decreased first and then increased with the increase of the experiment time after the direct current of 0.2-1.6 A was applied, respectively [18,19]. Qian et al. studied the corrosion behavior of spray painted pipe by direct current in simulated soil, and the experimental test results showed that the corrosion rate of pipe was linearly related to the amplitude of direct current density [20,21]. Dai et al. conducted relevant studies on the direct current corrosion of X52 steel in simulated soil solution and compared the direct current corrosion under cathodic protection [22,23]. The results showed that the direct current accelerated the dissolution process of anode iron and had a great influence on the integrity of the pipeline. For the cathode, the direct current will increase the pH of the cathode and may lead to the peeling of the coating on the pipeline surface. Muralidharan et al. studied the influence of direct current on the corrosion behavior of steel in simulated alternating dry-wet soil by means of weight loss method, electrochemical test, XRD and SEM [24]. The results showed that the corrosion rate of steel was higher in the case of direct current than in the case of no direct current. The larger the amplitude of direct current density was, the higher the corrosion rate of steels was. The study in reference [25] had reached the same conclusion.

Current studies showed that the corrosion rate was closely related to the direct current density, and the higher the direct current density was, the larger the corrosion rate was. However, the influence of the direct current field on the grounding electrode can not be ignored, especially for the UHVDC transmission system [26]. However, the direct current corrosion caused by faults was very rare. Under

normal operating conditions, the allowable unbalance current of UHVDC was no more than 1% of the rated current. In this paper, the  $\pm 800$  kV-UHVDC transmission with rated current of 5000 A was taken as an example to study the corrosion behavior of grounding electrode materials in the direct current field formed by unbalanced current during normal operation through electrochemical experiment and immersion experiment, which was of great significance for the prediction and protection of grounding material corrosion.

## 2. EXPERIMENT SETTINGS

Experimental schematic diagram was shown in Figure 1. The electrode material of the direct current power supply in the experiment was graphite, in which the length and width of the graphite electrode should be at least twice as that of the test samples, and the two graphite electrodes were 150 mm apart and arranged symmetrically. The detection part was an electrochemical test system, which was placed in the middle of two graphite plates, using a three-electrode system, including a reference electrode (RE) (saturated calomel electrode, SCE), an auxiliary electrode (AE) (platinum electrode, Pt), and a working electrode (WE) (Q345B steel, the main components were shown in Table 1). The reference electrode was in contact with the solution through a luggin capillary, and the tip of the luggin capillary was no more than 2 mm from the surface of the working electrode.

**Table 1.** Main chemical component in mass fraction (%) of Q345B steel

| C    | Si   | Mn   | P     | S     | Ni   | Cu   | Nb   | Ti   | Fe   |
|------|------|------|-------|-------|------|------|------|------|------|
| 0.18 | 0.43 | 1.36 | 0.027 | 0.024 | 0.41 | 0.22 | 0.03 | 0.11 | Bal. |

The surface of Q345B steel was successively cleaned by acetone, deionized and anhydrous ethanol, and then dried in the vacuum dryer for at least 24 h before experiment. The size of the Q345B steel was  $25 \times 25 \times 2$  mm<sup>3</sup>, and the welding wire was welded on a wide surface of the Q345B steel. The welding surface and four sides of the Q345B steel were encapsulated with epoxy resin and ethylenediamine, leaving another wide surface, namely the working surface, with an area of 625 mm<sup>2</sup>. The Q345B steel should be sealed to ensure that the welding points will not fall off and the epoxy material will not overflow to the working surface. The working surface was polished step by step with #800~#1200 waterproof sandpaper, to keep the working surface of the Q345B steel in mirror-like.

In order to more accurately and conveniently test the relevant parameters of Q345B steel under different direct current density, soil simulation solution was used to replace the actual soil as the corrosion solution medium based on the field test data. The experiment solution consisted of Cl<sup>-</sup> in 0.1 mol/L, SO<sub>4</sub><sup>2-</sup> in 0.1 mol/L and HCO<sub>3</sub><sup>-</sup> in 0.1 mol/L, which was prepared by the deionized water and analytical reagents.

The experiment device included direct current interference part and electrochemical testing part. In the direct current interference part, the stable tracking direct current power source (SS2323) generated stable direct current density of 0-1.5 A/cm<sup>2</sup> in corrosive environment, forming a stable and

controllable electric field. In the electrochemical testing part, the electrochemical workstation (PARSTAT2273) was used to test the change curves of working electrode under different direct current density, including open-circuit potential ( $E_{OCP}$ ) and polarization curves. It should be noted that the change of  $E_{OCP}$  within  $\pm 3\text{mV}$  in 300 s was considered to be in a stable condition and then the  $E_{OCP}$  was recorded for more than 10 min. The test range of polarization curve was  $\pm 250\text{ mV}$  (vs.  $E_{OCP}$ ) with the scanning rate of  $0.5\text{ mV/s}$ , and the change rules of related parameters including corrosion potential ( $E_{corr}$ ), corrosion current density ( $I_{corr}$ ), cathode Tafel constant ( $\beta_c$ ) and anode Tafel constant ( $\beta_a$ ) were obtained by PowerSuite software. The whole experimental device was put into constant temperature - humidity chamber (GDJS-408) to keep the experiment temperature at  $20^\circ\text{C}$ .

Immersion experiments under different experiment time and direct current density were carried out. After the experiment, the morphology of the corrosion products was observed by SEM and the composition of the corrosion products was analyzed by XRD to determine the reaction process under different direct current density. After removing the corrosion products, the corrosion rate and the maximum pit depth was calculated, and the corrosion morphology of Q345 steel was observed.

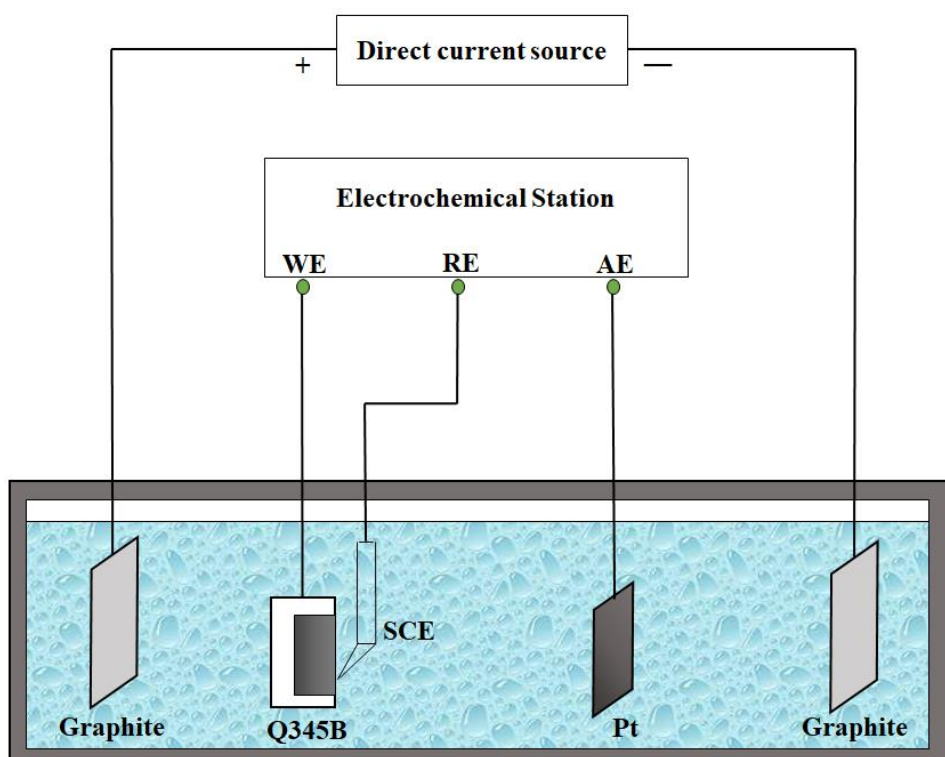


**Figure 1.** The experiment device for electrochemical tests including open-circuit potential ( $E_{OCP}$ ) and polarization curves of Q345B steel under the direct current density of  $0\text{-}1.5\text{ A/cm}^2$  in experiment solution at  $20^\circ\text{C}$

### 3. RESULTS AND DISCUSSION

#### 3.1 Electrochemical experiments

##### 3.1.1 Open-circuit potential ( $E_{\text{OCP}}$ )

The open-circuit potential ( $E_{\text{OCP}}$ ) was the potential at which the metal reached a stable corrosion state without an applied current. However, the corrosion rate of metal was not intrinsically related to the open-circuit potential, which only indicated that the more negative the open-circuit potential was, the greater the tendency of metal to be corroded will be. Considering the influence of applied direct current density on Q345B steel, the potential drop caused by solution resistance between reference electrode and working electrode was corrected by means of the off-potential [27], resulting in a more accurate open-circuit potential of Q345B steel under the different direct current density.

Figure 2 showed the open-circuit potential ( $E_{\text{OCP}}$ ) of Q345B steel under different direct current density ( $I_{\text{DC}}$ ). It can be concluded that the  $E_{\text{OCP}}$  of Q345B steel remained stable for a long time under different direct current density based on the stability criterion proposed in this paper. In addition, before the corrosion of Q345B reached stabilization, the  $E_{\text{OCP}}$  will decrease greatly [28]. As can be seen from the figure, when the applied direct current density was  $0.3 \text{ A/cm}^2$ , the  $E_{\text{OCP}}$  of Q345 steel became positive compared with that without direct current density, meaning that the corrosion tendency of Q345B steel became smaller at this time. When the direct current density was greater than  $0.3 \text{ A/cm}^2$  and then increased continually, the  $E_{\text{OCP}}$  of Q345B steel had a linear negative deviation, namely  $E_{\text{OCP}} = -0.00651 \cdot I_{\text{DC}} - 0.7469$  ( $R^2 = 0.9728$ ) [29,30]. Under this circumstance, the corrosion tendency of Q345B steel was greater, that is, the more easily to be corroded [31].

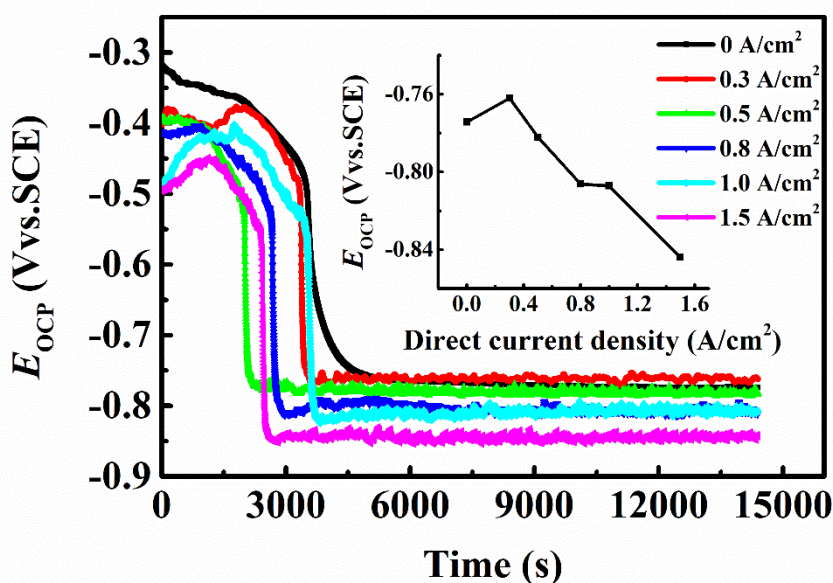


**Figure 2.** The open-circuit potential ( $E_{\text{OCP}}$ ) of Q345B steel under different direct current density of 0-1.5  $\text{A/cm}^2$  in experiment solution at  $20^\circ\text{C}$

3.1.2 Polarization curve

Figure 3 showed the polarization curves of Q345B steel under different direct current density. As can be seen from the figure, the effect of direct current on the cathodic polarization curve of the Q345B steel was more significant than that on the anodic polarization curve. Generally speaking, under this circumstance, the corrosion potential ( $E_{corr}$ ) of the Q345B steel shifted negatively with the increase of the direct current density [32].

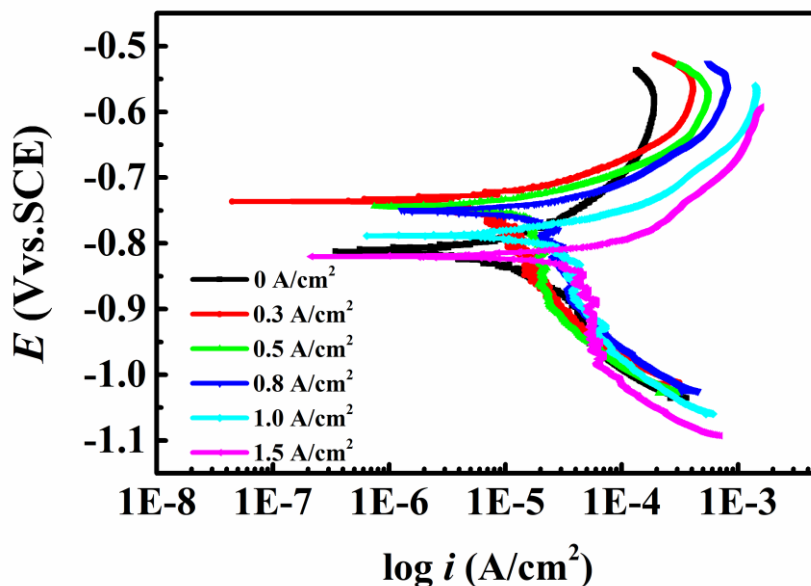


**Figure 3.** Polarization curves of Q345B steel under different direct current density of 0-1.5 A/cm<sup>2</sup> in experiment solution at 20°C

**Table 2.** Fitting parameters of polarization curves of Q345B steel under different direct current density of 0-1.5 A/cm<sup>2</sup> in experiment solution at 20°C

| $I_{DC}$ , A/cm <sup>2</sup> | $E_{corr}$ , V | $I_{corr}$ , $\mu$ A/cm <sup>2</sup> | $\beta_a$ , mV | $\beta_c$ , mV | $r = \beta_a/\beta_c$ |
|------------------------------|----------------|--------------------------------------|----------------|----------------|-----------------------|
| 0                            | -0.787         | 15.08                                | 123            | 97             | 1.275                 |
| 0.3                          | -0.739         | 8.284                                | 142            | 75             | 1.886                 |
| 0.5                          | -0.773         | 11.42                                | 184            | 74             | 2.494                 |
| 0.8                          | -0.789         | 18.00                                | 316            | 72             | 4.362                 |
| 1.0                          | -0.784         | 31.93                                | 351            | 53             | 6.608                 |
| 1.5                          | -0.817         | 46.79                                | 382            | 50             | 7.699                 |

However, when the direct current density was 0.3 A/cm<sup>2</sup> and 0.5 A/cm<sup>2</sup>, the  $E_{corr}$  was slightly more positive than that without the direct current density. Table 2 was the fitting results of polarization curves. With the increase of the direct current density, the anodic Tafel constant ( $\beta_a$ ) increased while the cathodic Tafel constant ( $\beta_c$ ) decreased, resulting in that the corrosion process gradually changed from mixed control to anodic control [33]. Compared with the corrosion potential ( $E_{corr}$ ) and corrosion current density ( $I_{corr}$ ) without the direct current density, the  $E_{corr}$  was more positive and the  $I_{corr}$  was

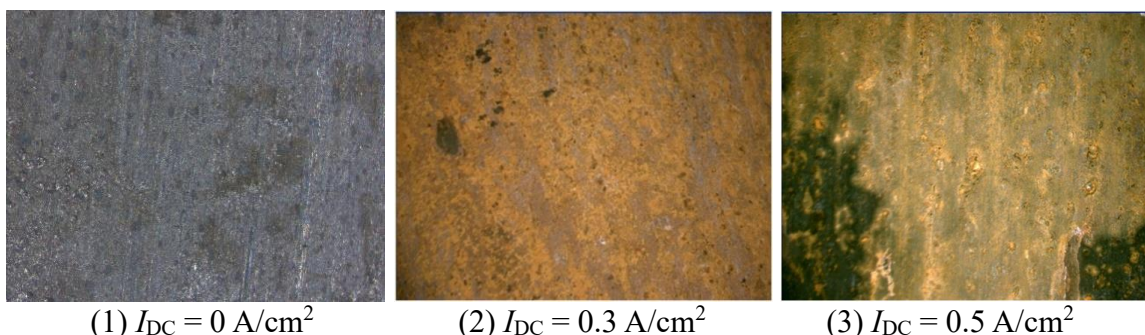
smaller at  $I_{DC} = 0.3 \text{ A/cm}^2$  and  $0.5 \text{ A/cm}^2$  [34-36]. Subsequently, as the direct current density continued to increase, the  $E_{corr}$  deviated negatively, namely  $E_{corr} = -0.0568 \cdot I_{DC} - 0.7338$  ( $R^2 = 0.8784$ ), while the  $I_{corr}$  increased significantly, namely  $I_{corr} = 33.69 \cdot I_{DC} - 4.3406$  ( $R^2 = 0.9649$ ) [37].

### 3.2 Immersion experiment

#### 3.2.1 Corrosion product

Figure 4 showed the morphology of corrosion product of Q345B steel under different direct current density. As can be seen from the figure, there was no obvious dense corrosion products on the surface of Q345B steel without direct current density. When the direct current density ( $I_{DC} = 0.3 \text{ A/cm}^2$ ) was applied, it can be seen from the figure that pale brown corrosion product layer was generated on the surface of Q345 steel, and the structure of the corrosion product layer was relatively intact. With the increase of direct current density, the corrosion product layer still showed good integrity. As the direct current density continued to increase, the color of corrosion products gradually changed from pale brown to brown. When the direct current density was  $1.0 \text{ A/cm}^2$ , the corrosion products were basically brown. However, when the direct current density reached  $1.5 \text{ A/cm}^2$ , the corrosion product layer on the surface of Q345B steel became incomplete and granular [38].

Therefore, in view of the above changes in corrosion products, XRD and the micro morphology of corrosion product particles were used to analyze the surface reaction process changing with the direct current density. The results were shown in Figure 5 and Figure 6. When the direct current density was  $0.3 \text{ A/cm}^2$ , the corrosion products were mainly  $\text{Fe}_2\text{O}_3$  ( $\text{FeO(OH)} \rightarrow \text{Fe}_2\text{O}_3 + \text{H}_2\text{O}$ ) and  $\text{FeO(OH)}$  ( $4\text{Fe} + 3\text{O}_2 + 2\text{H}_2\text{O} \rightarrow 4\text{FeO(OH)}$ ) [39], which basically covered the surface of Q345B steel. When the direct current density was  $0.8 \text{ A/cm}^2$  and  $1.5 \text{ A/cm}^2$ , the corrosion products were mainly  $\text{Fe}_2\text{O}_3$ ,  $\text{FeO(OH)}$  and  $\text{FeCO}_3$  ( $\text{Fe} + \text{HCO}_3^- \rightarrow \text{FeCO}_3 + \text{H}^+ + 2\text{e}^-$ ) [40]. Furthermore, the  $\text{FeCO}_3$  content at  $I_{DC} = 1.5 \text{ A/cm}^2$  was significantly higher than that at  $I_{DC} = 0.8 \text{ A/cm}^2$ . Therefore, with the increase of direct current density, the coverage rate of corrosion products on the surface of Q345B steel gradually decreased, and the corrosion products changed from polygon to triangle [41]. Combined with the results of corrosion potential ( $E_{corr}$ ) and corrosion current density ( $I_{corr}$ ), the corrosion tendency and corrosion rater at  $I_{DC} = 0.3 \text{ A/cm}^2$  and  $0.5 \text{ A/cm}^2$  was slighter than that at  $I_{DC} = 0 \text{ A/cm}^2$ , which was due to the relatively complete corrosion product layer on the surface of Q345B steel at  $I_{DC} = 0.3 \text{ A/cm}^2$  and  $0.5 \text{ A/cm}^2$ .



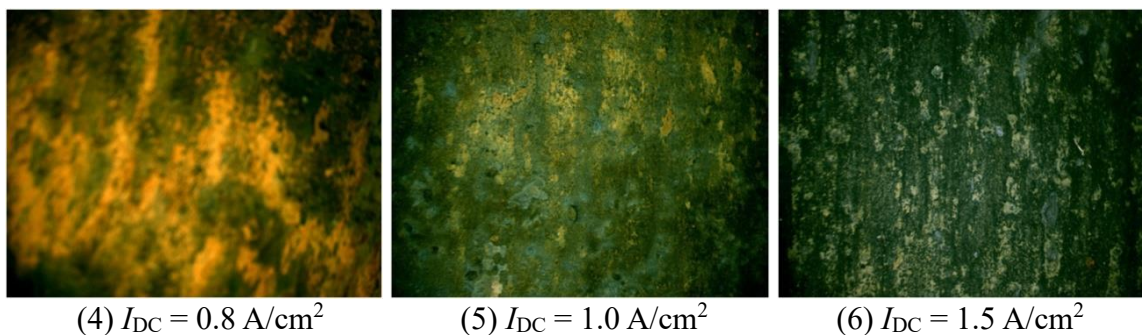


**Figure 4.** Morphology of corrosion product of Q345B steel under different direct current density of 0-1.5 A/cm<sup>2</sup> in experiment solution at 20°C

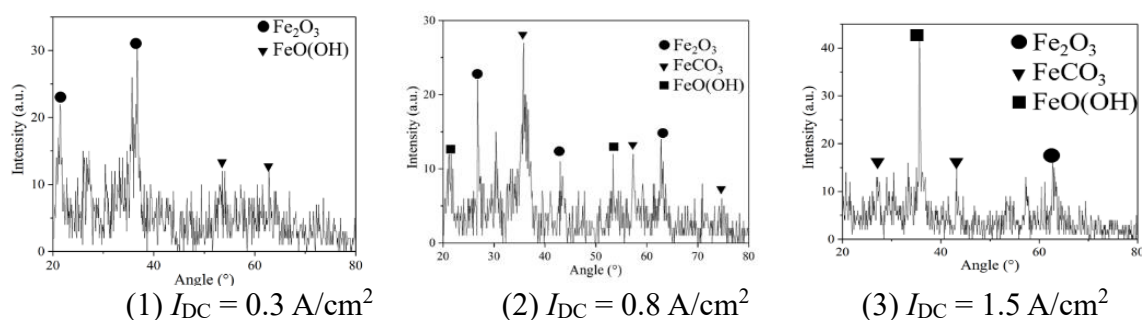


**Figure 5.** XRD analysis of corrosion product of Q345B steel under different direct current density of 0-1.5 A/cm<sup>2</sup> in experiment solution at 20°C

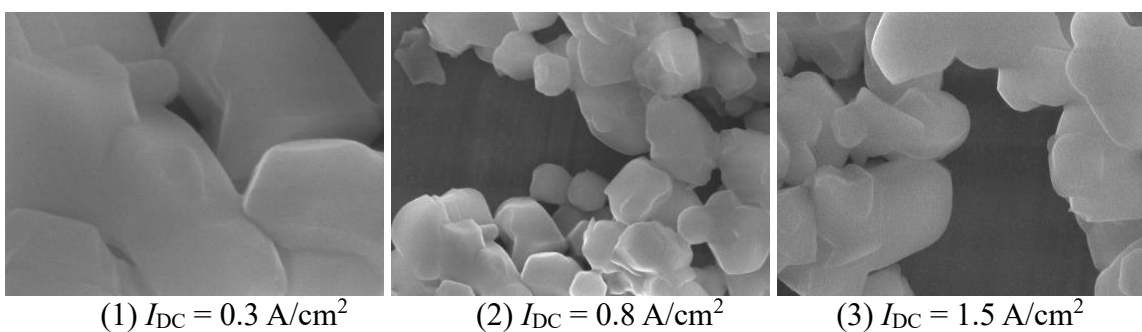


**Figure 6.** Micro morphology of corrosion product of Q345B steel under different direct current density of 0-1.5 A/cm<sup>2</sup> in experiment solution at 20°C (×5000)

### 3.2.2 Corrosion rate

Figure 7 showed the corrosion rate of Q345B steel with time under different direct current density. Under different experimental time, the change of corrosion rate was very small and can be ignored, in which the error may be caused by the incomplete treatment of corrosion products and water absorption of epoxy resin [42]. From another aspect, in the same experiment time, the larger the direct current density was, the higher the corrosion rate was. This was because the corrosion process of Q345B steel under different direct current density was mainly controlled by the anode process, and its corrosion rate was mainly related to the movement speed of electrons [43]. Time accumulation may

affect the layer morphology of corrosion products on the surface of Q345B steel, but had no effect on the general corrosion rate. Therefore, according to the above characteristics, the corrosion rate under the different direct current density was averaged and its standard deviation was calculated. There was a good linear relationship between the corrosion rate and the direct current density, namely corrosion rate =  $0.0648 \cdot I_{DC} + 0.0047$  ( $R^2=0.9952$ ) [44]. According to the standard deviation of the corrosion rate at different experiment times, it can be considered that the corrosion rate was not affected by the experiment time. In essence, under the anodic control, electrochemical corrosion of Q345B steel followed the Faraday's law, thus the corrosion rate was proportional to the amount of electricity per unit time [45]. Therefore, it can be further inferred that under the interference of direct current density, the corrosion rate of metal was only related to the direct current density, and had nothing to do with the environment [46].

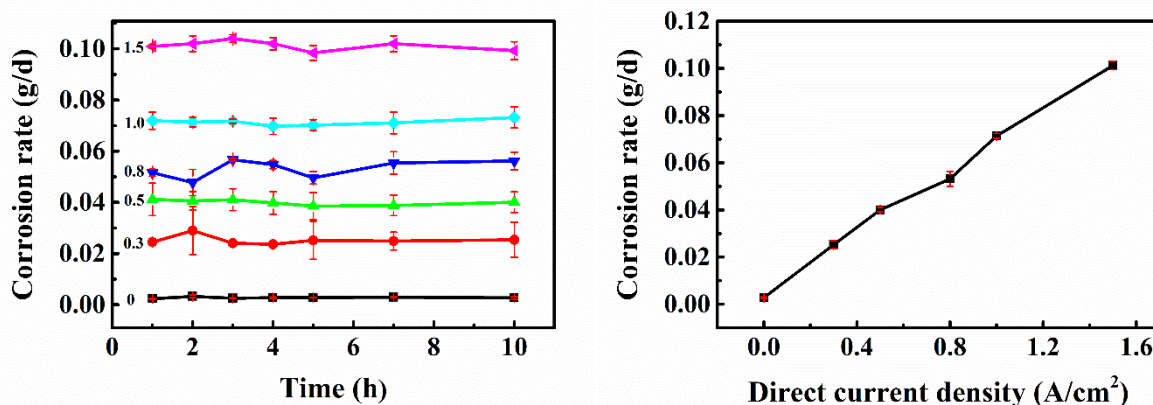
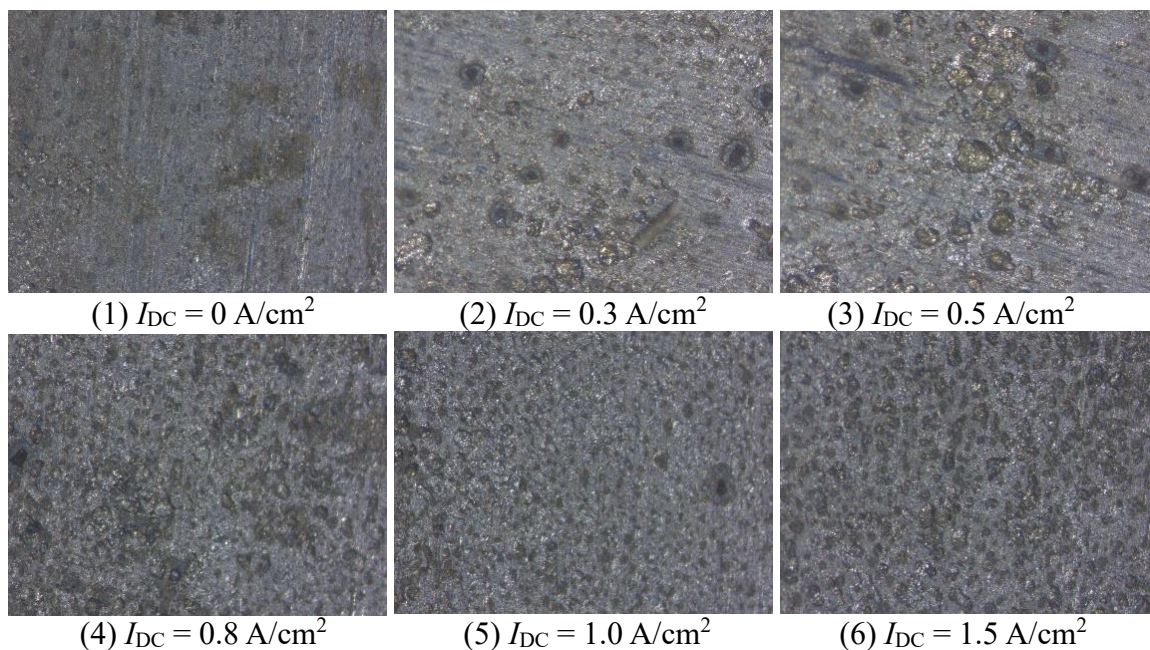


**Figure 7.** Corrosion rate of Q345B steel with time under different different direct current density of 0-1.5 A/cm<sup>2</sup> in experiment solution at 20°C

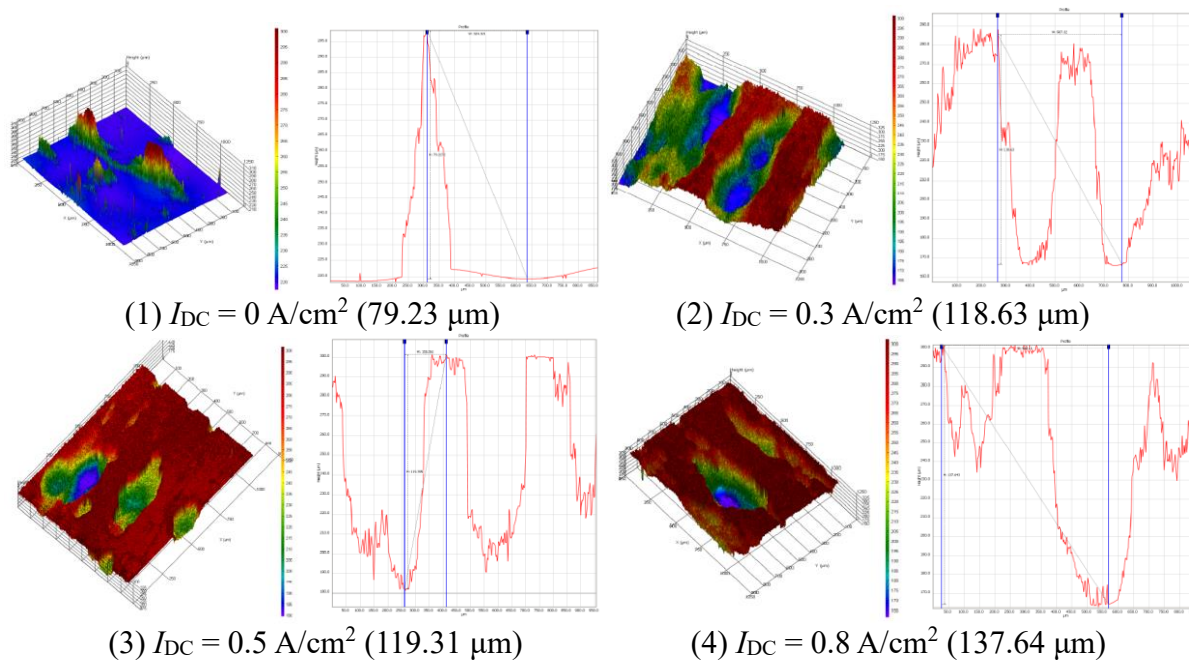
### 3.2.3 Maximum pit depth

Figure 8 showed the corrosion morphology of Q345B steel under different direct current density. As can be seen from the figure, with the increase of direct current density, the number of corrosion pits on the surface of Q345 steel gradually increased. Compared with the condition of no direct current density, there were large and obvious pitting pits formed on the surface of Q345B steel at  $I_{DC} = 0.3$  A/cm<sup>2</sup> and 0.5 A/cm<sup>2</sup>. With the increase of direct current density, pitting pits were more dense and obvious located on the surface of Q345B steel at  $I_{DC} = 0.8-1.5$  A/cm<sup>2</sup> [47]. Combined with the analysis of the morphology of corrosion products in Section 3.2.1, it can be seen that with the increase of the direct current density, the corrosion products on the surface of Q345B steel gradually became granular, which almost had no effect on the corrosion process of Q345B steel [48]. The maximum pit depth of Q345B steel under different direct current density was analyzed, as shown in Figure 9. It can be seen that with the increase of direct current density, the maximum pit depth of Q345B steel increased gradually, namely maximum pit depth =  $80.032 \cdot I_{DC} + 83.946$  ( $R^2=0.9554$ ) [49]. In addition, at  $I_{DC} = 0.3$  A/cm<sup>2</sup> and 0.5 A/cm<sup>2</sup>, the maximum pit depth was basically the same, which

was because the corrosion product layer can completely cover the Q345B surface at this time, reducing the erosion of the surface by the corrosive medium such as  $\text{Cl}^-$  [50].



**Figure 8.** Corrosion morphology of Q345B steel under different direct current density of 0-1.5  $\text{A}/\text{cm}^2$  in experiment solution at  $20^\circ\text{C}$



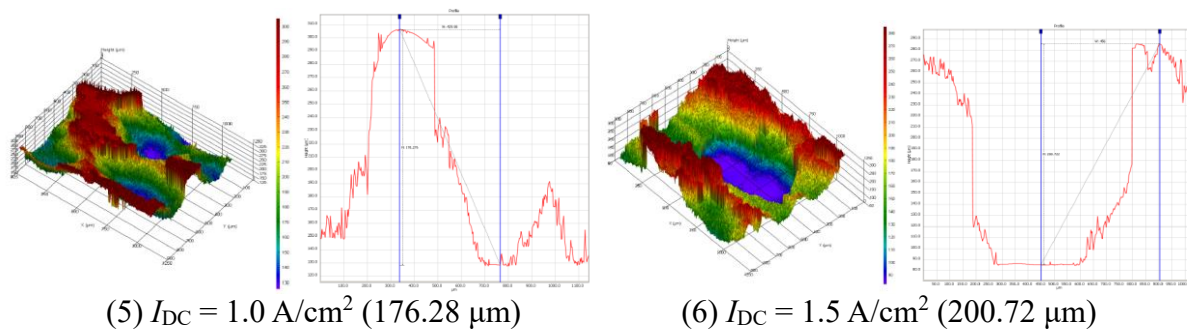


**Figure 9.** Maximum pit depth of Q345B steel under different direct current density of 0-1.5 A/cm<sup>2</sup> in experiment solution at 20°C

#### 4. CONCLUSIONS

In this paper, the corrosion behavior of Q345B steel as grounding electrode material was studied under different direct current density based on the electrochemical experiment and immersion experiment. The following conclusions were drawn.

(1) With the increase of direct current density ( $I_{DC}$ ), the corrosion potential ( $E_{corr}$ ) of Q345B steel deviated negatively, namely  $E_{corr} = -0.0568 \cdot I_{DC} - 0.7338$  ( $R^2 = 0.8784$ ), while the corrosion current density ( $I_{corr}$ ) increased significantly, namely  $I_{corr} = 33.69 \cdot I_{DC} - 4.3406$  ( $R^2 = 0.9649$ ). Meanwhile, the corrosion process gradually changed from mixed control to anodic control.

(2) With the increase of direct current density, the coverage rate of corrosion products on the surface of Q345B steel gradually decreased, and the corrosion products changed from polygon to triangle, including  $\text{Fe}_2\text{O}_3$  ( $\text{FeO}(\text{OH}) \rightarrow \text{Fe}_2\text{O}_3 + \text{H}_2\text{O}$ ),  $\text{FeO}(\text{OH})$  ( $4\text{Fe} + 3\text{O}_2 + 2\text{H}_2\text{O} \rightarrow 4\text{FeO}(\text{OH})$ ) and  $\text{FeCO}_3$  ( $\text{Fe} + \text{HCO}_3^- \rightarrow \text{FeCO}_3 + \text{H}^+ + 2\text{e}^-$ ).

(3) With the increase of direct current density, there were good linear relationship between the corrosion rate / maximum pit depth and the direct current density, namely corrosion rate =  $0.0648 \cdot I_{DC} + 0.0047$  ( $R^2 = 0.9952$ ) and maximum pit depth =  $80.032 \cdot I_{DC} + 83.946$  ( $R^2 = 0.9554$ ), respectively.

#### ACKNOWLEDGEMENT

This paper was a periodical achievement of the 2020 Science and Technology Research Project of Department of Education of Hubei Province, China, "Research and design of intelligent rotary stereo garage" (Grant No. B2020358).

#### References

1. S. Chandrasekar, C. Kalaivanan, A. Cavallini and G. Montanari. *IEEE T. on Dielect. El. In.*, 16 (2009) 574.
2. F. Zhang, L. Bing, G. Wang, Y. Liao and L. Ling. *IEEE T. on Dielect. El. In.*, 22 (2015) 2937.
3. L. Ling, L. Wang, Z. Guan, F. Zhang and L. Li. *IEEE T. on Dielect. El. In.*, 22 (2015) 2242.

4. P. Han, G.F. Qiao, B.B. Guo, D.S. Li and J.P. Ou. *Int. J. Elec. Power.*, 134 (2022) 107436.
5. E.A. Cherney, A.C. Baker, J. Kuffel and Z. Lodi. *IEEE T. Power Deliver.*, 29 (2014) 275.
6. F. Zhang, L. Bing, G. Wang, Y. Liao and L. Ling. *IEEE T. on Dielect. El. In.*, 22 (2015) 2937.
7. D.M. Yang, B. Cao, Z. Li, L.W. Yang and Y.K. Wu. *Int. J. Elec. Power.*, 131 (2021) 107097.
8. S.J. Ma, Y.X. Du, K. Che, H.M. Qin and Y.J. Su. *Mater. Corros.*, 73 (2022) 540.
9. H.M. Qin, Y.X. Du, M.X. Lu and Q.S. Meng. *Mater. Corros.*, 71 (2020) 35.
10. Y.X. Du, H.M. Qin, J. Liu and D.Z. Tang. *Mater. Corros.*, 72 (2021) 1038.
11. H.M. Qin, Y.X. Du, M.X. Lu, X.P. Sun and Y. Zhang. *Mater. Corros.*, 71 (2020) 1856.
12. M. Iwata, T. Ohtaka, Y. Goda, S. Yamagami, A. Kato and K. Nagano. *Electr. Eng. Jpn.*, 214 (2021) e23345.
13. S. Wang, Y.B. Hu, Z.Z. Li, S.J. Gao and X.G. Li. *Corrosion*, 12 (2013) 357.
14. G. Doyle, M.V. Seica and M.W. *Can. Geotech. J.*, 40 (2003) 225.
15. P. Peng, X.J. Zeng, Y. Leng, K. Yu and Y.R. Ni. *IEEE T. Electr. Electr.*, 15 (2020) 1482.
16. K. Yu, Y.R. Ni, X.J. Zeng, P. Peng, X.Y. Fan and Y. Leng. *IEEE T. Electr. Electr.*, 15 (2020) 1507.
17. I.S. Cole and D. Marney. *Corros. Sci.*, 56 (2012) 5.
18. A. Mujezinović, S. Martinez and K. Kekez. *Mater. Corros.*, 70 (2019) 357.
19. B. Zhang, F.Y. Cao, X.B. Meng, Y.L. Liao and R.H. Li. *IET Gener. Transm. Dis.*, 12 (2018) 1177.
20. S. Qian and Y.F. Cheng. *Constr. Build. Mater.*, 148 (2017) 675.
21. S. Qian and Y.F. Cheng. *Constr. Build. Mater.*, 261 (2020) 120550.
22. N.W. Dai, Q.M. Chen, J.X. Zhang, X. Zhang and Q.Z. Ni. *Mater. Chem. Phys.*, 192 (2017) 190.
23. N.W. Dai, J.X. Zhang, Q.M. Chen, B. Yi, F.H. Cao and J.Q. Zhang. *Corros. Sci.*, 99 (2015) 295.
24. S. Muralidharan, D.K. Kim, T.H. Ha, J.H. Bae, Y.C. Ha, H.G. Lee and J.D. Scantlebury. *Desalination*, 216 (2007) 103.
25. Z.R. Zhang, Z. Xu and T. Xu. *J. Mod. Power Syst. Cle.*, 4 (2016) 300.
26. E.Z. Juybari, R. Keypour and M. Niasati. *IET Electr. Syst. Tran.*, 11 (2021) 322.
27. X.B. Liu, M.Y. Xia, D. Bolati, J.P. Liu, Q. Zheng and H. Zhang. *Energy Sci. Eng.*, 8 (2020) 248.
28. H. Zhang and Y.X. Du. *Electrochemistry*, 88 (2020) 1726.
29. R. Alipio, M. Guimares, L. Passos, D. Conceio and M.T.C.D. Barros. *Electr. Pow. Syst. Res.*, 20 (2017) 1830.
30. H.L. Huang, X.P. Guo, G.A. Zhang and Z.H. Dong. *Corros. Sci.*, 53 (2011) 3446.
31. H.L. Huang, Z.Q. Pan, X.P. Guo and Y.B. Qiu. *T. Nonferr. Metal. Soc.*, 24 (2014) 285.
32. X. Zhang, J.X. Zhang, N.W. Dai, Y. Yang, X.J. Yuan, F.H. Cao and J.Q. Zhang. *Mater. Chem. Phys.*, 206 (2018) 232.
33. Z. Zhang, J. Zou, Y. Dan, H. Ye and J. Deng. *IET Gener. Transm. Dis.*, 14 (2020) 1730.
34. S. Antonio, S. Lillard, P. Dragan, M. Rubinstein and F. Rachidi. *Electr. Pow. Syst. Res.* 34 (2019) 1530.
35. B.Y. Ku and J.S. Liu. *IET Gener. Transm. Dis.*, 14 (2020) 1.
36. S. Yu, H. Jin and M.F. Cao. *Constr. Build. Mater.*, 347 (2022) 128631.
37. X. Peng, Z.Q. Huang, B. Chen, D.M. Liu and H.K. Li. *Eng. Fail. Anal.*, 116 (2020) 104760.
38. J.G. Feng, Z.G. Chen, C. Wu, C.K. Qin, X.S. Wei. *Process Saf. Environ.*, 164 (2022) 38.
39. M.R. Dayyari, A. Amadeh and S. Sadreddini. *Mater. Chem. Phys.*, 199 (2017) 537.
40. W.L. Cai, S.J. Xie, C. Jomdecha, X.J. Wang, C.X. Pei, Y. Li, Z.M. Chen and N. Yusa. *Corros. Sci.*, 123 (2017) 197.
41. S. Yu, H. Jin and M.F. Cao. *Constr. Build. Mater.*, 347 (2022) 128631.
42. H. Jin and S. Yu. *Constr. Build. Mater.*, 272 (2021) 121646.
43. K.H. Ryu, T.H. Lee, J.H. Kim, S. Hwang, N.Y. Lee, J.H. Kim, J.H. Park and C.H. Sohn. *Nucl. Eng. Des.*, 240 (2010) 468.
44. C.T. Wang, W. Li, G.F. Xin, Y.Q. Wang, S.Y. Xu and M.B. Fan. *Measurement*, 200 (2022) 111592.
45. E.Z. Zhou, F. Li, D.W. Zhang, D.K. Xu, Z. Li, R. Jia, Y.T. Jin, H. Song, H.B. Li, Q. Wang, J.J. Wang, X.G. Li, T.Y. Gu, A.M. Homborg, J.M.C. Mol, J.A. Smith, F.H. Wang and D. R. Lovley.

*Water Res.*, 219 (2022) 118553.

46. Z.P. Chen, L. Gao and D.A. Koleva. *Measurement*, 196 (2022) 111217.

47. J.R. Qin and M. Curioni. *Electrochim. Acta*, 428 (2022) 140927.

48. W.Q. Xu, Y. Li, H.Z. Li, K. Wang, C.P. Zhang, Y.B. Jiang and S. Qiang. *Constr. Build. Mater.*, 314 (2022) 125618.

49. K.K. Tang. *Mater. Today. Commun.*, 20 (2019) 100564.

50. I. Aldellaa, P. Havlásek, M. Jirásek and P. Grassl. *Eng. Fract. Mech.*, 264 (2022) 108310.

© 2022 The Authors. Published by ESG ([www.electrochemsci.org](http://www.electrochemsci.org)). This article is an open access article distributed under the terms and conditions of the Creative Commons Attribution license (<http://creativecommons.org/licenses/by/4.0/>).